Continental Shelf Research 61–62 (2013) 23–30

Contents lists available at SciVerse ScienceDirect

Continental Shelf Research

journal homepage: www.elsevier.com/locate/csr

Research papers

Variability in nitrogen sources for new production in the vicinity of the shelf edge of the East China Sea in summer

Xin Liu [a,b], Ken Furuya [a,*], Takuhei Shiozaki [a], Takako Masuda [a], Taketoshi Kodama [a], Mitsuhide Sato [a], Hitoshi Kaneko [c], Maki Nagasawa [c], Ichiro Yasuda [c]

[a] Department of Aquatic Bioscience, The University of Tokyo, Yayoi, Bunkyo, Tokyo 113-8657, Japan
[b] College of the Environment and Ecology, Xiamen University, Xiamen 361005, China
[c] Atmosphere and Ocean Research Institute, The University of Tokyo, Kashiwa, Chiba 277-8564, Japan

ARTICLE INFO

Article history:
Received 15 November 2012
Received in revised form
14 February 2013
Accepted 3 April 2013
Available online 22 April 2013

Keywords:
New nitrogen
Turbulent nitrate flux
N_2 fixation
Internal wave
Vertical mixing

ABSTRACT

The relative importance of new nitrogen sources for primary production was investigated in well stratified subtropical waters in the vicinity of the shelf edge of the East China Sea by concurrent determinations of upward turbulent nitrate flux across the pycnocline, nitrate assimilation, N_2 fixation and primary production. On the coastal side of the Kuroshio jet close to the shelf edge, strong vertical diffusivity K_ρ was observed. The half-day mean K_ρ at the top nitracline was 3.9×10^{-5} m^2 s^{-1}. Consequently, a higher turbulent upward nitrate flux of 445 μmol N m^{-2} d^{-1} across the nitracline was observed than that of 82 μmol N m^{-2} d^{-1} off the shelf near the Kuroshio jet and 146 μmol N m^{-2} d^{-1} on the slope at the outer side of the Kuroshio jet. This high upward flux supported the highest rates of primary production (27.3 mmol C m^{-2} d^{-1}) and nitrate assimilation (764 μmol N m^{-2} d^{-1}), and the contribution of the upward nitrate flux to new nitrogen was 5.7 times higher than that of N_2 fixation. In contrast, N_2 fixation was a major new nitrogen source at stations off the shelf, where the upward nitrate flux was less evident due to less vertical diffusivity and weaker vertical nitrate gradients than near the shelf break in the Kuroshio jet. These observations demonstrate that new nitrogen sources were highly variable according to relative locations at the shelf edge and Kuroshio jet in the East China Sea and the adjacent waters during summer.

1. Introduction

On the basis of the source and form of nitrogen, primary production can be partitioned into new and regenerated production (Dugdale and Goering, 1967). Furthermore, new production is considered to be balanced with export production, which can be removed from the surface mixed layer as fish yields and the export of particulate organic matter to the deep ocean (Eppley and Peterson, 1979). Export production is supported by newly available nitrogen, including turbulent upward nitrate flux due to vertical mixing, with N species transported by horizontal and vertical advections, atmospheric nitrogen deposition, and N_2 fixation. In a warm and vast tropical and subtropical ocean, phytoplankton biomass is low because of the scarcity of nutrients caused by strong water column stratification.

Turbulent nitrate vertical flux across the pycnocline, therefore, has traditionally been considered to be a dominant mechanism of nitrogen supply to the euphotic zone (McCarthy and Carpenter, 1983). In contrast, the significance of N_2 fixation on new production in oligotrophic waters has become well recognized recently (Capone et al., 2005; Shiozaki et al., 2009; Mouriño-Carballido et al., 2011). Mouriño-Carballido et al. (2011) measured N_2 fixation and nitrate turbulent diffusion concurrently in the Atlantic Ocean, and revealed that N_2 fixation could equal or even exceed the input of turbulent nitrate flux in this oligotrophic region. Moreover, they demonstrated that these two processes varied considerably at different spatio-temporal scales, which were induced by a variety of biogeochemical processes.

The East China Sea (ECS) is a marginal sea of the Pacific Ocean that includes a large area of the shallow continental shelf and oligotrophic Kuroshio current, and is one of the most studied areas associated with nutrient cycling in the world (Chen et al., 2003a). Chen and Wang (1999) evaluated nutrient mass balance in the ECS and concluded that the nitrate input from the Kuroshio subsurface and intermediate water to shallow waters on the expansive shelf is the most important source.

However, it is only partially understood how nutrients in subsurface and intermediate waters are supplied to the euphotic zone. To date physical processes responsible for the nitrate supply have been proposed including upwelling in the northwest of

* Corresponding author. Tel.: +81 3 5841 5293; fax: +81 3 5841 5308.
E-mail address: furuya@fs.a.u-tokyo.ac.jp (K. Furuya).

0278-4343/$ - see front matter © 2013 Elsevier Ltd. All rights reserved.
http://dx.doi.org/10.1016/j.csr.2013.04.014

Taiwan, frontal eddies along the Kuroshio, tidal mixing, internal waves, and typhoons (Yanagi et al., 1998; Chen et al., 1999, 2001, 2003b; Chen and Chen, 2003; Kanda et al., 2003; Matsuno et al., 2005, 2009). However, the relative importance of these processes is poorly understood. Other than physical processes, the role of N_2 fixation on the biogeochemical cycles in the ECS has not been well studied until recently. Thus, N_2 fixation in the ECS as well as in the neighboring waters has not been considered as a new nitrogen source. However, recent studies demonstrated that active N_2 fixation occurred in the oligotrophic region of the ECS (Shiozaki et al., 2010; Zhang et al., 2012), indicating that N_2 fixation would significantly contribute to new production.

In the present study, we present the first simultaneous measurements of the upward nitrate flux across the pycnocline, nitrate assimilation, N_2 fixation and primary production at the shelf edge of the ECS and the adjacent waters. On the basis of previous studies to determine the variability of nitrogen sources for new production in the northwestern Pacific, three stations were selected to represent three sub-areas: near the shelf edge and the Kuroshio jet in the ECS, off the shelf near the Kuroshio jet in the ECS, and in the subtropical water on the continental slope east of the Ryukyu Islands with little influence from the Kuroshio.

2. Materials and methods

2.1. Study site

Field observations were carried out in the ECS and the adjacent area (Fig. 1) during the R/V Tansei-maru KT-10–19 cruise from 4 to 12 September, 2010. Primary production, N_2 fixation and nitrate assimilation were determined at Stn 1 off the shelf near the Kuroshio front, Stn 4 at the shelf edge near the Kuroshio front, and Stn 7 in the subtropical waters on the slope. Stn 1 (30°39.6′N, 129°11.6′E, 560 m depth) was located about 80 km from the adjacent shelf edge represented by the 200 m bathymetric contour (Fig. 1) and in the frontal zone just north of the Kuroshio jet with the mean current velocity of (0.8 m s^{-1}, 84° from RDI-shipboard ADCP) at 20 m depth observed during 0:00–12:00 UTC on September 4 when the age of the moon was about 25 just after the neap tide. Stn 4 (28°24.3′N, 126°54.2′E, 280 m depth) was located near the shelf edge and in the frontal zone just north of the Kuroshio jet with the mean current velocity of (0.75 m s^{-1}, 34°) at 20 m depth observed during 23:40 Sept. 8–17:52 Sept. 9 UTC when the age of the moon was about 1 at the spring tide. Stn 7 (24°36.2′N, 125°44.9′E, 950 m depth) was located south of Ryukyu Island Chain 23:06 Sept. 10–17:24 Sept. 11 UTC when the age of the moon was about 3 just after the spring tide. Abundant *Trichodesmium* and high N_2 fixation rates were reported in the vicinity of Stns 1 and 4 (Marumo and Asaoka, 1974; Shiozaki et al., 2010), and Stn 7 was located also in a high N_2 fixation area near Miyako-jima Island (Shiozaki et al., 2010). Since internal tides are generated near the shelf edge and along the Ryukyu Archipelago (Niwa and Hibiya, 2004), vertical mixing can be induced which promotes turbulent nitrate flux across the pycnocline for new production in the vicinity of Stns 4 and 7 (Sharples et al., 2001). Therefore, Stns 1, 4 and 7 were chosen to examine the relative importance of N_2 fixation and turbulent nitrate flux as nitrogen sources for new production.

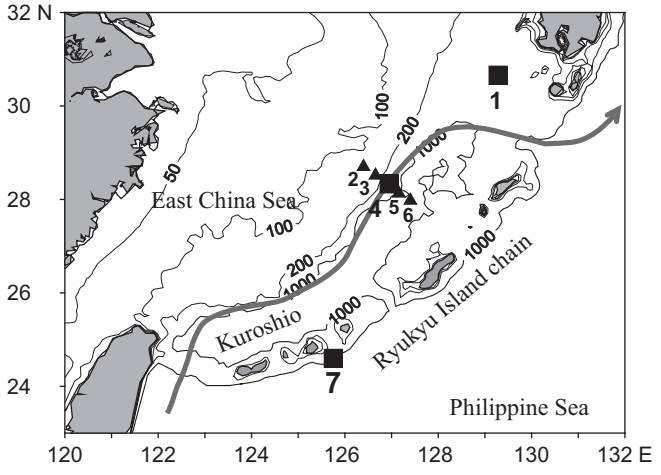

Fig. 1. Sampling stations in the East China Sea and its adjacent area. Solid squares indicate three 12-h time series stations. An arrow shows the Kuroshio path on September 9, 2010 (⟨http://www1.kaiho.mlit.go.jp/KANKYO/KAIYO/qboc/⟩).

2.2. Nutrients and Chl a

Temperature and salinity were profiled using a Seabird SBE 911 CTD and water sampling was made using Niskin bottles mounted on a carrousel fitted with the CTD. Water samples for nutrients and chlorophyll (Chl) *a* were collected from 10 to 12 layers in the upper 200 m water column.

Samples for nutrients analysis were collected in duplicate acid-cleaned polypropylene bottles (50 or 100 mL) and were kept frozen until analysis on land. Concentrations of nitrate, nitrite, and soluble reactive phosphorus were first determined by a conventional colorimetric method. When nutrient concentrations were <0.1 μM, samples were analyzed at the nanomolar level on land using a highly sensitive colorimetric system that consisted of an AutoAnalyzer II (Technicon) connected to a liquid waveguide capillary cell (World Precision Instruments) (Hashihama et al., 2009). The detection limit was 3 nM for both nitrate plus nitrite and soluble reactive phosphorus.

For fluorometric determination of Chl *a* using a Turner Design 10-AU fluorometer, seawater samples were filtered onto 25 mm Whatman GF/F filters and Chl *a* was extracted in N, N-dimethylformamide (Suzuki and Ishimaru, 1990).

2.3. Incubation experiments

The euphotic zone was defined as the upper water column down to the depth at which the downward photosynthetically active radiation (PAR) was 1% of the value just below the surface. Vertical profiles of light intensity (PAR) were obtained at each station using a free-fall spectroradiometer (SPMR, Satlantic), just prior to water sampling.

Water samples for nitrate assimilation were collected from 100%, 50%, 25%, 10%, and 1% light depths, and introduced into duplicated acid-cleaned 2 L polycarbonate bottles. ^{15}N-labeled nitrate (99.8 at% ^{15}N; Shoko) was spiked into each bottle to give the final tracer concentrations of 10 nM. For samples collected from the 1% light depth, 100 nM, 200 nM and 20 nM of ^{15}N-nitrate were spiked at Stns 1, 4 and 7, respectively, according to nutrient analyses conducted during previous cruises in the study area. Bottles were subsequently wrapped in neutral-density screens to adjust each light level, and then incubated in an on-deck incubator cooled by running surface seawater. The incubations were made from 00:00 to 12:00 h local time and terminated within 2 to 3 h to minimize complications due to cycling and potential depletion of nutrients (McCarthy et al., 1996, 1999). At the beginning of the incubation, subsamples (4.5 L) were filtered onto precombusted GF/F filters to estimate the initial ^{15}N enrichment of particulate organic nitrogen. Detailed procedures for the pretreatment and analysis have been described elsewhere (Shiozaki et al., 2009). Since nitrate was depleted above the nitracline where nitrate exceeded 1 μM (Shiozaki et al., 2011), the addition of ^{15}N-nitrate

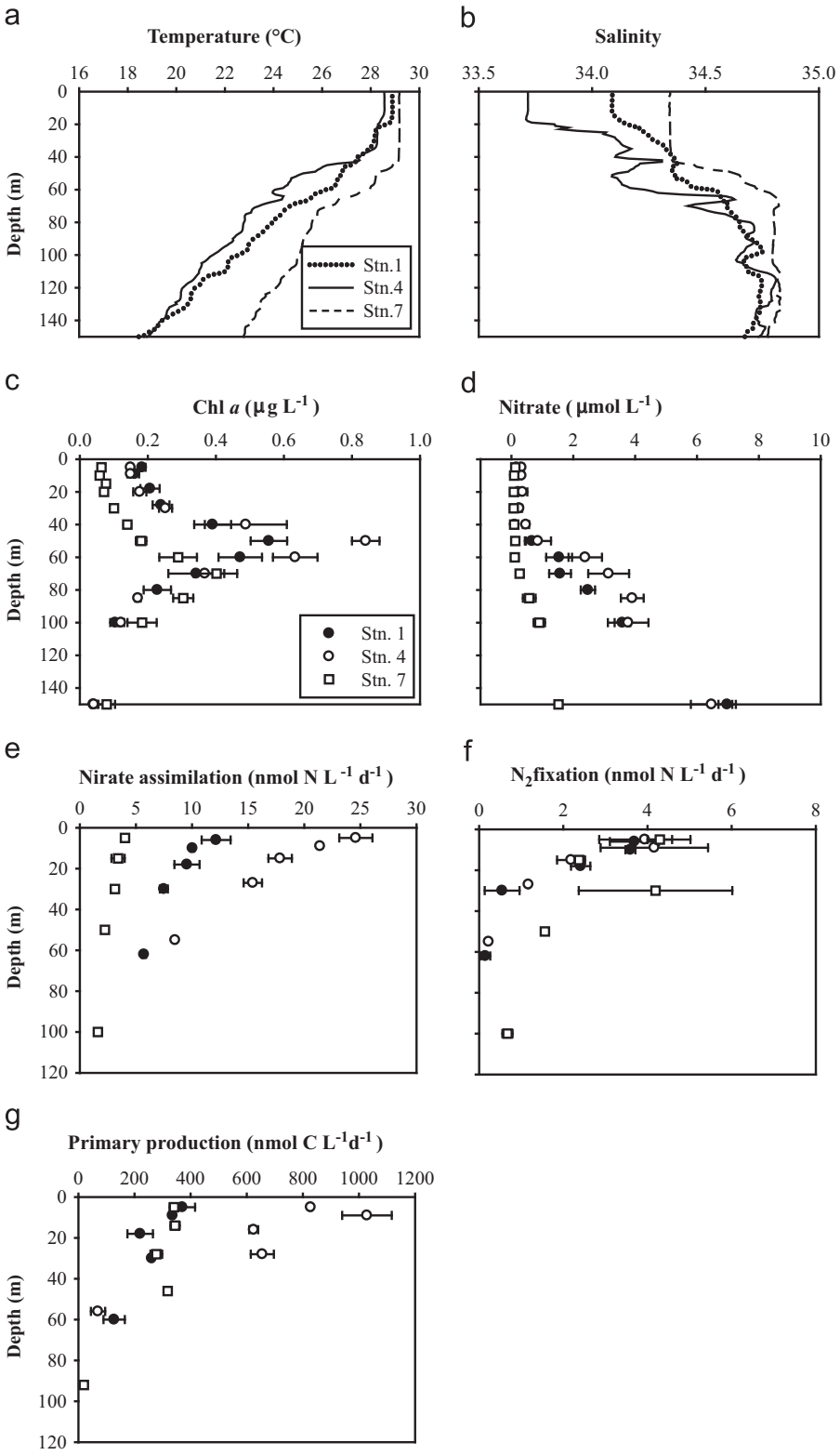

Fig. 2. Vertical profiles of temperature (a), salinity (b), chlorophyll *a* (c, μg L^{-1}) nitrate concentrations (d) and of nitrate assimilation (e), N_2 fixation rates (f) and primary production (g) at Stns 1, 4, and 7 on September 4, 9, and 11, 2010, respectively. Error bars represent the standard errors during the 12-h time series observations (a–d) and half the difference between duplicate measurements (e–g). The deepest samples of panels e–g were collected from the 1% light depth.

could overestimate nitrate assimilation. Therefore, the in situ rates were corrected by assuming that the in situ nitrate assimilation rates at ambient nitrate concentrations were lower by the same percentage as the measured rates based on our previous study on nitrate assimilation in this region using Michaelis–Menten kinetics (Shiozaki et al., 2011). Since the light and dark periods were approximately 12:12 during the cruise, daily rates of nitrate assimilation (*R*, nmol N m^{-2} d^{-1}) were computed by summing the

uptake for both day and night using Eq. 1 (Shiozaki et al., 2009):

$$R = R_0 \times 12 + R_{12} \times 12 \quad (1)$$

where R_0 and R_{12} represented the ratios measured at 00:00 and 12:00 h, respectively.

N_2 fixation and primary production were measured by a dual isotopic labeling by ^{15}N and ^{13}C (Shiozaki et al., 2009). Duplicate samples were collected from the same light depths as nitrate assimilation and introduced into acid-cleaned 4.5 L polycarbonate bottles. ^{13}C-labeled sodium bicarbonate (99 at% 13C; Cambridge Isotope Laboratories) was added to each bottle to achieve a final tracer concentration of 200 μM before sealing it with a thermoplastic elastomer cap. Then, using a gas-tight syringe, 2 mL of $^{15}N_2$ gas (99.8 at% ^{15}N; Shoko) was added to each bottle. The bottles were incubated in an on-deck incubator for 24 h. Before the measurements of the $^{14}N/^{15}N$ ratio in the particulate organic nitrogen samples, we conducted a precision test using a standard gas to confirm that the errors on the isotopic composition were $< \pm 0.05‰$ (Montoya et al., 1996). Rates of N_2 fixation and primary production were calculated using the equations proposed by Montoya et al. (1996) and Hama et al. (1983), respectively.

2.4. Vertical diffusivity and turbulent nitrate flux

Direct turbulence measurements of mm-scale velocity shear were conducted in the upper 500 m water column using a VMP500 (Rockland Scientific, Canada) in order to estimate turbulent energy dissipation rates and vertical diffusivities. The VMP500 was a tethered free-falling vertical profiler with two shear probes and pumped standard CTD sensors (SBE-3 and SBE-4, Sea-Bird Electronics). Sampling rates of the shear sensors and SBE-CTD were 512 and 64 Hz, respectively. Influences of instrumental noise and disturbance of the main body were removed from the shear data, which were then divided into 16 s segments (approximately equivalent to 10 m depth segments) overlapping by 14 s. The kinetic energy dissipation rate, ε was calculated from the integral of the shear spectrum in each segment, yielding data at 1 m intervals.

The profiler was repeatedly cast 5 times at 3 h intervals within a half-day to cover the semi-diurnal tide that is the dominant tidal constituent. Vertical eddy diffusivity K_ρ ($m^2\ s^{-1}$) was calculated using the following equation (Osborn, 1980):

$$K_\rho = \lambda\varepsilon/N^2 \quad (2)$$

where N (s^{-1}) is the Brunt–Väisälä frequency obtained by the VMP500-equipped CTD, and λ is the mixing efficiency, which was taken to be 0.2 (Osborn, 1980). Turbulent nitrate flux, F (in μmol N $m^{-2}\ d^{-1}$) was calculated using K_ρ and the vertical nitrate gradient ($\partial NO_3^-/\partial z$) (μmol m^{-4}) at the nitracline on the basis of the Fickian diffusion theory (Eq. (3)).

$$F = -K_\rho\ \partial NO_3^-/\partial z \quad (3)$$

The 95% confidence intervals for the N, ε, K_ρ, $\partial NO_3^-/\partial z$, and F in each stations were calculated by the bootstrap method (Efron and Gong, 1983).

In the present estimate of new nitrogen sources, we assumed a steady state that the nitrate supplied was instantaneously consumed by phytoplankton because the surface nitrate was almost completely depleted. We also excluded nitrate supply of upwelling associated with heaving isopycnal surfaces due to frontal eddies etc. Although turbulent nitrate flux N_2 fixation and nitrate assimilation rates estimated in the present study are all indispensable processes to evaluate nitrogen circulations, we need further studies including other sources such as upwelling.

3. Results

3.1. Hydrographic conditions, Chl a and nutrients

Distinct vertical patterns of temperature, salinity, Chl *a* and nitrate were observed at Stns 1, 4, and 7 showing a thermally well stratified water column (Fig. 2). Both nitrate and phosphate were undetectable in the upper 40 m at all stations using conventional nutrient analysis (Fig. 2d). Different water masses were distributed among the three stations in the upper 150 m ($< 24\sigma$) (Fig. 3). A distinction between the ECS upper water (Stns 1 and 4) and the Philippine Sea upper water (Stn 7) was obvious in the *T–S* diagrams (Fig. 3). Typical characteristics of vertical nitrate profiles in the northwest Philippine Sea (Kodama et al., 2011) appeared at Stn 7, including strong stratification, a deep mixed layer down to around 50 m, a subsurface Chl *a* maximum layer located at 100 m, and the least steep vertical gradient of nitracline ($\sim$30 μmol m^{-4}) among the three stations (Fig. 2d). On the other side of Kuroshio, Stns 1 and 4 were characterized by a shallower mixed layer down to around 20 m, with a relatively shallow nitracline located around 60 m, and a shallower subsurface Chl *a* maxima (Fig. 2). Compared with Stn 1, Stn 4 showed complicated structures in both the thermocline and halocline with vertical temperature and salinity inversions (Figs. 2 and 3). The inversions were reported to be caused by intrusions of low-salinity shelf water into the Kuroshio thermocline along the shelf edge due to baroclinic instability of the Kuroshio current (Isobe et al., 2004). A lower temperature observed from 40 to 100 m at Stn 4 coincided with a higher Chl *a* maximum at 50 m and nitrate concentration at 80 m (Fig. 2). It is thus not surprising that the nitracline was shallower in the ECS with a steeper vertical gradient in the nitracline (> 100 μmol m^{-4}) located around 60 m. It is noted that considerable variations in nitrate concentration within 12 h were observed at depths ranging from 50 to 100 m at Stn 4, near the shelf edge of the ECS (Fig. 2d).

3.2. Vertical profiles of turbulent energy dissipation (ε), Brunt–Väisälä frequency (N) and vertical diffusivity (K_ρ)

Vertical profiles of the turbulent kinematic energy dissipation rate (ε) representing turbulent intensity, squared Brunt–Väisälä frequency (N^2), and vertical diffusivity (K_ρ) were estimated every 3 h for a half day (Fig. 4). Compared with Stn 1, Stns 4 and 7 had many significant vertical structures that were found using the observations of N^2 and ε (Fig. 4). The magnitude of ε varied vertically between O (10^{-10}) and O (10^{-6}) W kg^{-1}, while a strong turbulent dissipation was found frequently around 60 and 200 m, having a magnitude sometimes exceeding O (10^{-7}) W kg^{-1} (Fig. 4). The shallow peaks of ε found in the upper layer at Stns 4 and 7 were located in the upper part of the thermocline (60 m), which was coincident with a relatively large Brunt–Väisälä frequency (Fig. 4b and c). The largest ε occurred below 170 m at Stn 4 just above the bottom of the shelf edge ($\sim$250 m). While at Stns 1 and 7 whose bottom depth was 600 and 970 m, respectively, a large ε was found around 200 m and located in the intermediated layer. The ε at the nitracline of Stns 4 and 7, was 3.9 and 2.8×10^{-8} W kg^{-1}, respectively, and tended to be higher than at Stn 1 (1.0×10^{-8} W kg^{-1}). Coincidently, the K_ρ showed similar vertical distribution patterns to ε. Large values of K_ρ were found frequently around 30, 60, and 200 m, with the magnitude exceeding $10^{-4}\ m^2\ s^{-1}$. Values at 150 m were less than the order of $10^{-5}\ m^2\ s^{-1}$. At the nitracline at Stns 4 and 7, the half-day means of K_ρ were 3.9 and $3.5 \times 10^{-5}\ m^2\ s^{-1}$, respectively, which were higher than those at Stn 1 ($0.9 \times 10^{-5}\ m^2\ s^{-1}$) as well. Although the magnitudes of K_ρ in the nitracline of all the three stations were still on the order of $10^{-5}\ m^2\ s^{-1}$, relatively larger values observed at Stns 4 and 7 were located at depths just above the K_ρ peaks with the magnitude exceeding $10^{-4}\ m^2\ s^{-1}$ (Fig. 4b and c).

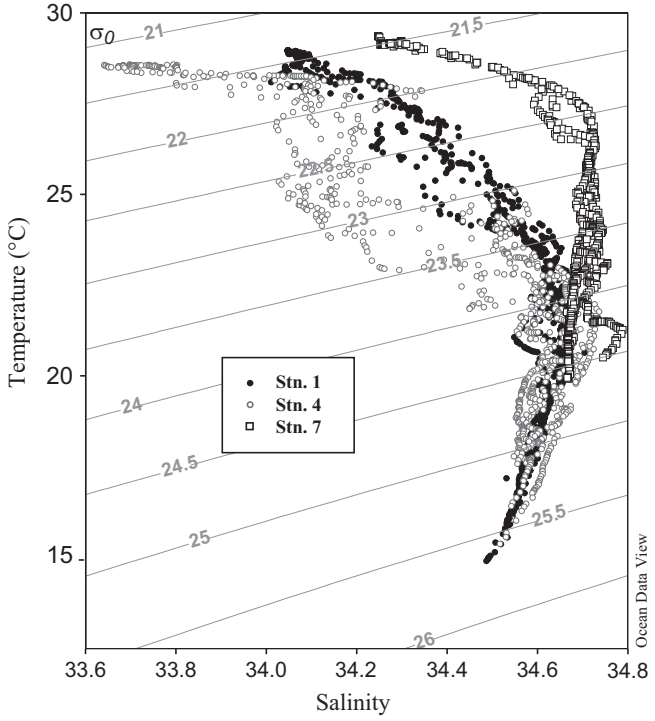

Fig. 3. *T/S* diagram at Stns 1, 4 and 7 on September 4, 9, and 11, 2010, respectively.

3.3. Turbulent nitrate flux and associated primary production, N_2 fixation and nitrate assimilation rates

Turbulent nitrate flux varied considerably within 12 h (Table 1). The large variations in the turbulent nitrate flux were mainly caused by fluctuations in vertical diffusivity at these three stations (C.V. mean = 132%). In general, the maximum vertical nitrate flux resulted from large values of K_ρ, which were one or two orders of magnitude higher than those with low vertical nitrate flux. Near the sources of large internal tides as in the SCS (e.g. Niwa and Hibiya, 2004), 1–2 order of magnitude variability of vertical diffusivity has been commonly observed (e.g. Matsuno et al., 2005). At Stn 4, the maximum turbulent nitrate flux of 1542 μmol N m^{-2} d^{-1} (Table 1) was associated with the lowest nitrate gradient, but the largest K_ρ at the nitracline. Temporal variations in turbulent nitrate flux were high especially at Stns 4 and 7, ranging over two orders of magnitude (Table 1).

The vertical maximum of N_2 fixation and nitrate assimilation occurred at the surface and/or the 50% light depth (Fig. 2e and f). The highest nitrate assimilation rate was observed at the surface of Stn 4 with 25 nmol N L^{-1} d^{-1}, while it was 12 and 4 nmol N L^{-1} d^{-1} at the surface of Stns 1 and 7, respectively (Fig. 2e). The depth-integrated daily nitrate assimilation down to the 1% light depth at Stn 4 was up to 764 μmol N m^{-2} d^{-1} (Table 2). Coincidently, primary production was maximum at the 50% light depth at Stn 4 with 1028 nmol C L^{-1} d^{-1}, which was twice that at the other two stations. Depth-integrated primary production at these three stations were 13, 27, and 21 mmol C m^{-2} d^{-1}, and N_2 fixation rates were 70, 79, and 179 μmol N m^{-2} d^{-1}, at Stns 1, 4 and 7, respectively (Table 2).

A high nitrate gradient ($\partial NO_3^-/\partial z$) and K_ρ at the nitracline (~62 m) were found at Stn 4 with 153 μmol m^{-4} and 3.9×10^{-5} m^2 s^{-1}, respectively (Table 2). Therefore, turbulent nitrate mixing across the nitracline (445 μmol N m^{-2} d^{-1}) became strong at this station. The turbulent nitrate flux substantially exceeded the N_2 fixation at Stn 4 (Table 2). Although K_ρ at the nitracline of Stns 4 and 7 was of the same order of magnitude (Table 1), the turbulent nitrate flux at Stn 7 was lower

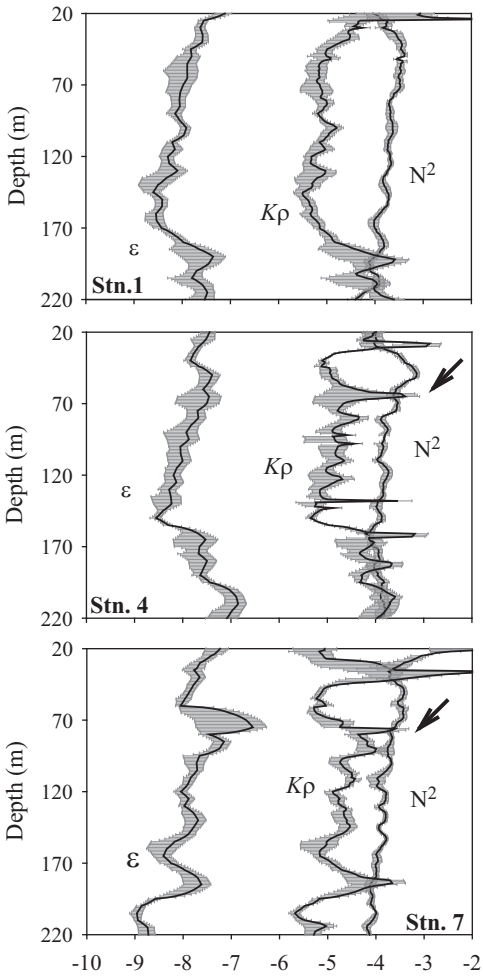

Fig. 4. Vertical profiles of vertical diffusivity (K_ρ, m^2 s^{-1}), turbulent energy dissipation rate (ε, W kg^{-1}) and Brunt–Väisälä frequency (N^2, s^{-2}) at Stns 1, 4, and 7, respectively. Gray error bars represent the standard errors during the 12 h time series observations. Black arrows indicate peaks of K_ρ observed around the nitracline. The *X*-axes is a logarithmic scale.

(145 μmol N m^{-2} d^{-1}) than at Stn 4 (445 μmol N m^{-2} d^{-1}) due to the lower nitrate gradient (29 μmol N m^{-4}) at the nitracline at Stn 7 (Tables 1 and 2). The vertical diffusivity at the nitracline at Stn 1 was relatively lower than at Stns 4 and 7 (Table 1). Therefore, vertical turbulent nitrate flux was low at Stn 1 (Table 2). The turbulent nitrate fluxes at Stns 1 and 7 were comparable to N_2 fixation values.

4. Discussion

4.1. Variability of turbulence intensity and turbulent nitrate flux

There was considerable variation in microstructure in the mixed layer and the thermocline in our study area. Compared with Stn 1, Stns 4 and 7 showed distinct vertical microstructures of Brunt–Väisälä frequency, where large ε values below 50 m corresponded to the strong vertical diffusivity. The elevated K_ρ near the surface might be attributed to the turbulence induced by wind stress (Matsuno et al., 2006). In contrast, the distinct peak of ε and K_ρ near the bottom at 170–220 m at Stn 4 corresponded to the bottom boundary layer (Fig. 4b) as reported by Han et al. (2001) and Matsuno et al. (2005, 2009). Previous studies suggest that these large ε values above the bottom are induced by bottom stress due to tidal currents, resulting in a distinct bottom mixed layer with a high K_ρ (Matsuno et al., 2005). This process was used to

Table 1
Brunt–Väisälä frequency (N^2), turbulent energy dissipation rate (ε), vertical diffusivity (K_ρ), nitrate gradients ($\partial NO_3/\partial z$) and turbulent nitrate flux at nitracline depths at Stns. 1, 4 and 7, respectively. Nitracline depth corresponds to the depth of the 1 μM isoline. Numerals in parentheses denote 95% CI.

Stn	Local Time	N^2	ε	K_ρ	$\partial NO_3/\partial z$	Nitrate diffusion
		($\times 10^{-4}$, s^{-2})	($\times 10^{-8}$, W kg^{-1})	($\times 10^{-5}$, m^2 s^{-1})	(μmol N m^{-4})	(μmol N m^{-2} d^{-1})
1	0:00	2.1	0.2	0.2	168	32
	3:00	4.8	0.4	0.2	104	14
	6:00	1.3	0.6	1	51	44
	9:00	2.0	0.7	0.7	143	88
	12:00	2.6	3.0	2.3	117	232
	Mean	2.6 (1.6–3.9)	1.0 (0.3–2.3)	0.9 (0.2–1.8)	116 (77–152)	82 (26–177)
4	0:00	0.6	4.5	14	124	1542
	3:00	3.7	1.8	1	175	150
	6:00	8.8	11	2.6	164	364
	9:00	4.1	1.0	0.5	145	62
	12:00	1.8	0.7	0.8	159	109
	Mean	3.8 (1.5–6.7)	3.9 (1.0–8.6)	3.9 (0.7–11.0)	153 (134–170)	445 (86–953)
7	0:00	1.8	0.1	0.1	24	2
	3:00	1.7	0.6	0.8	18	12
	6:00	1.6	3.3	4.1	18	64
	9:00	1.5	9.0	12	61	631
	12:00	2.3	0.7	0.6	26	14
	Mean	1.8 (1.6–2.1)	2.8 (0.4–6.8)	3.5 (0.4–9.0)	29 (20–50)	145 (8–474)

Table 2
Mean and their 95% CI of depths of the nitracline and euphotic zone bottom, each corresponding to the depth of the 1 μM nitrate isoline and 1% of the PAR just below the surface, respectively. Chl *a* concentration, nitrate assimilation, N_2 fixation and primary production were integrated from the surface down to the base of the euphotic layer (1% light depth of the surface PAR). TF:TN is the ratio of turbulent nitrate flux (TF) to N_2 fixation (NF).

	Stn 1	Stn 4	Stn 7
Nitracline (m)	66 (60–75)	62 (55–79)	127 (101–150)
Euphotic zone depth (m)	58 (49–67)	56 (54–57)	93 (83–102)
Chl *a* (mg m^{-2})	18 (15–21)	18 (15–21)	15 (12–16)
Turbulent nitrate flux (μmol N m^{-2} d^{-1})	82 (26–177)	445 (86-953)	146 (8–474)
Nitrate assimilation (μmol N m^{-2} d^{-1})	412	764	217
N_2 fixation (μmol N m^{-2} d^{-1})	70	79	179
Primary production (mmol C m^{-2} d^{-1})	12.6	27.3	20.6
TF:NF	1.2	5.6	0.81

explain an offshore intrusion that is sometimes observed as a high-turbidity tongue in the subsurface water of the Kuroshio (Matsuno et al., 2009). Interactions between rough topography and strong Kuroshio currents may enhance diffusivity at a larger extent from bottom and thus near-surface biological layer (Nikurashin and Ferrari, 2010). On the other hand, it has been suggested that the large ε found around the thermocline is related to internal waves, which depend strongly on Brunt–Väisälä frequency (Fig. 4b and c). Matsuno et al. (2005) reported that the distinct maxima of the ε values detected around the thermocline were located at depths of the fine-scale shear maxima observed by the moored ADCP. Further, the maxima of ε found in the intermediate layer of Stns 1 and 7 around 200 m (Fig. 4a and c) may be attributed to the propagation of the vertically high wave number internal tides along the characteristic ray (Matsuno et al., 2005).

Stns 4 and 7 were located near the shelf break of the ECS and ridges along the Ryukyu Archipelago respectively. These narrow areas are located on either side of the Kuroshio jet, where internal waves were frequently observed (Kuroda and Mitsudera, 1995; Liu et al., 1998; Han et al., 2001; Park et al., 2006). Using a two-dimensional analytical model, Baines (1982) predicted that the slope of the continental shelf in the ECS and its adjacent area is the second largest generator of the M_2 internal tides among the major continental shelf slopes in the world's oceans. Indeed, a series of studies revealed that internal waves intermittently generated around the shelf break of the ECS and the ridges along the Ryukyu Archipelago could induce enhanced vertical mixing. Consequently, it has been hypothesized that this process may support new production (Kuroda and Mitsudera, 1995; Matsuno et al., 1997, 2005; Han et al., 2001; Lee et al., 2006; Park et al., 2006). Repeated hydrographic surveys across the shelf break showed that the vertical structure formed by an intensified thermocline and bottom or intermediate mixed layer could change daily (Han et al., 2001). Further, Matsuno et al. (2005) showed intermittent intensification of the vertical mixing associated with internal waves on the basis of measurements of the microscale structure around the shelf break of the ECS. Approximately 10% of the energy in the M_2 surface tide incident on prominent topographic features is converted to the M_2 internal tide, and approximately half of the M_2 internal tidal energy is subject to local dissipation in close proximity to the generation sites (Niwa and Hibiya, 2004). Thus, intensified turbulent nitrate flux might be attributed to the strong vertical shear and large dissipation induced by the internal waves that are generated at the continental shelf edge and ridges along the Ryukyu Archipelago. Furthermore, the largest turbulent nitrate flux was estimated at Stn 4, as enhanced vertical diffusivity and a steeper nitrate gradient were also observed there (Table 1). All these results indicate that the new nitrate from deeper water was brought into the euphotic zone by wave-induced turbulence, especially at the shelf edge in the ECS.

Despite relatively strong vertical diffusivity, the turbulent nitrate flux along the Ryukyu Archipelago cannot be considered as important as that at the shelf edge in the ECS. Diffusivities at the nitracline at these two stations are of the same order of magnitude

(Table 2), and integrated baroclinic energy conversion along the Ryukyu Archipelago (9.3 GW) is even higher than that at the shelf break of the ECS (4.1 GW) (Niwa and Hibiya, 2004). However, a significantly lower nitrate gradient was observed at the nitracline at Stn 7 (Figs. 2c and d, Table 2). Previous studies also revealed that the vertical gradient of the nitracline is steepest in the East China Sea followed by the Kuroshio Current and the least steep in the Philippine Sea (Kodama et al., 2011; Shiozaki et al., 2011).

This aerial difference in the gradient could be associated with the permanent thermocline depth. The 15 °C isotherm was located at around 200 m at Stns 1 and 4 near the Kuroshio jet, while it was around 400 m at Stn 7 east of the Ryukyu Islands. Correspondingly, thicker near surface water with low nitrate concentrations east of the Ryukyu Islands than at Stns 1 and 4, could lead to a weaker nitrate vertical gradient than at Stn 1 and 4. Thus, the impact of internal waves on the turbulent nitrate flux could be weakened by the gentle nutrient gradient in the water column near the Ryukyu Archipelago.

4.2. New nitrogen sources in the ECS and the adjacent area

The regional and seasonal variability of new production in the ECS and the adjacent area has been examined. The nitrate assimilation rates were significantly higher near the coast than the rates in the off-shelf areas due to the higher ambient nitrate concentrations (Chen et al., 1999, 2001; Kanda et al., 2003). Off-shelf in the ECS, nitrate in the surface water is depleted, and the assimilation rates become low (Kanda et al., 2003). The nitrate assimilation rate in this study area is therefore recognized to be significantly related to the ambient nitrate concentration. Consequently, any potential change from the nitrate sources in the off-shelf area would have an important impact on the nitrate assimilation rate. In the present study, the enhanced nitrate assimilation and primary production would be promoted by turbulent vertical nitrate flux near the shelf edge (Stn 4) as mentioned above. However, at the same time, nitrate assimilation rates exceeded the vertical nitrate flux at Stns 1 and 4 (Table 2). Especially at Stn 1, there was a marked discrepancy between the nitrate assimilation rate and the turbulent vertical nitrate flux. This imbalance was recognized previously (Shiozaki et al., 2011). Shiozaki et al. (2011) reported that the discrepancy increases 10-fold on the shelf of the ECS, with smaller discrepancies in adjacent, deep water regions of the Kuroshio and Philippine Sea, and hypothesized that the generation of nitrate by nitrification might play an important role, as abundant archaeal *amoA* were detected in the euphotic zone. Hence our observed imbalance might be partially due to nitrification. In addition, atmospheric deposition and advective fluxes induced by river plume, frontal eddies, and tides on the shelf of the ECS could also contribute to the high nitrate assimilation (Chen et al., 2003a, 2003b; Nakamura et al., 2005; Kodama et al., 2011; Zhao and Guo, 2011).

A recent study demonstrated that N_2 fixation rate determined by $^{15}N_2$ gas bubble injection method (Montoya et al., 1996) underestimate actual rates (Mohr et al., 2010). Furthermore, the bubble injection method can cause different degrees of underestimation of N_2 fixation according to diazotrophs composition (Grokopf et al., 2012). Thus, it is uncertain how much degree our rates underestimated N_2 fixation rates. To avoid the uncertainty, we regard our measured values as the most underestimated rates, that is, actual rates are considered to be higher than our estimates. N_2 fixation rates at Stns 1 and 7 were comparable with the turbulent nitrate flux (Table 2), indicating that N_2 fixation plays a critical role in new production at these stations. The stable nitrogen isotope of nitrate and of particulate organic nitrogen also indicate prevalent biological N_2 fixation in the outer shelf of the ECS (Minagawa and Wada, 1986; Liu et al., 1996; Minagawa et al., 2001), and support our results. Active N_2 fixation can be caused by a relatively high supply of the possibly limiting nutrients (Fe and/or P) for N_2 fixation from rivers and atmospheric inputs (Hashihama et al., 2009; Shiozaki et al., 2010).

Trichodesmium is considered to be a key diazotroph for evaluating N_2 fixation in seawater in our study region (Marumo and Asaoka, 1974; Chen et al., 2008; Shiozaki et al., 2010). It was observed by microscope in surface water samples at Stns 1, 4 and 7, with abundances of 6, 72 and 24 filaments L^{-1}, respectively. Although abundance of *Trichodesmium* at Stn 4 was higher than at Stn 7, N_2 fixation activity was not correlated with the abundance, which might indicate that their activity was suppressed by relatively high nitrate input at Stn 4. A recent study demonstrated that *Trichodesmium* become abundant in northwestern New Zealand where internal waves frequently occur (Stevens et al., 2012). Stevens et al. (2012) suggested that advective processes associated with internal waves caused floating material to aggregate at the surface and hence caused *Trichodesmium* patchiness. Enhanced vertical diffusivity and enhanced abundance of *Trichodesmium* at Stns 4 and 7 may be related with enhanced internal waves.

5. Conclusions

A large amount of energy in the M_2 surface tide is converted to the M_2 internal tide near the shelf edge of the ECS and approximately half of it could be subjected to local dissipation, which contributes to the mixing process (Niwa and Hibiya, 2004). Therefore, intensified turbulent mixing observed near the continental shelf edge of the ECS might be related to internal tides. Considerable variations in nitrate concentration, vertical diffusivity were observed at the depth of the nitracline at the shelf edge. Consequently, the highest turbulent nitrate flux (445 μmol N m^{-2} d^{-1}) occurred across the nitracline at the shelf edge, which resulted in the highest rates of primary production and nitrate assimilation (Table 2). In contrast, the highest N_2 fixation rate was observed in the vicinity of Miyako-jima Island. Taking into account the potential underestimation by the bubble injection method, new production by N_2 fixation in this area would exceed turbulent nitrate flux. Thus, new nitrogen sources are variable according to the location in the vicinity of the shelf edge of the ECS. Atmospheric deposition and nitrification as well as riverine inputs of terrestrial nitrogen are considered to be important as new nitrogen sources in the present study area, while these were not examined in the present study. Understanding the configuration of nitrogen sources and its controlling mechanism is a crucial next step to clarify the function of the biological pump in the highly dynamic shelf edge area of the interface of the ECS and the Kuroshio.

Acknowledgments

We express our sincere thanks to Paul J. Harrison for his helpful comments. Thanks are also to the captains, crew and scientists on board the R/V Tansei–maru cruise for their cooperation at sea. This research was financially supported by MEXT Grants-in-Aid for Scientific Research on Priority Areas (21014006), on Innovative Areas (24121001) and on (S20221002).

References

Baines, P.G., 1982. On internal tide generation models. Deep-Sea Research 29, 307–338.

Chen, Y.L.L., Chen, H.Y., 2003. Nitrate-based new production and its relationship to primary production and chemical hydrography in spring and fall in the East China Sea. Deep-sea Research Part II—Topical Studies in Oceanography 50, 1249–1264, http://dx.doi.org/10.1016/S0967-0645(03)00021-3.

Chen, Y.L.L., Chen, H.Y., Lee, W.H., Hung, C.C., Wong, G.T.F., Kanda, J., 2001. New production in the East China Sea, comparison between well-mixed winter and stratified summer conditions. Continental Shelf Research 21, 751–764.

Chen, C.T.A., Liu, K.K., Macdonald, R., 2003a. Continental margin exchanges. In: Fasham, M.J.R. (Ed.), Ocean Biogeochemistry. Springer-Verlag, Berlin, German, pp. 53–98.
Chen, C.T.A., Liu, C.T., Chuang, W.S., Yang, Y.J., Shiah, F.K., Tang, T.Y., Chung, S.W., 2003b. Enhanced buoyancy and hence upwelling of subsurface Kuroshio waters after a typhoon in the southern East China Sea. Journal of Marine Systems 42, 65–79, http://dx.doi.org/10.1016/S0924-7963(03)00065-4.
Chen, Y.L.L., Lu, H.B., Shiah, F.K., Gong, G.C., Liu, K.K., Kanda, J., 1999. New production and *f*-ratio on the continental shelf of the East China Sea: comparisons between nitrate inputs from the subsurface Kuroshio current and the Changjiang River. Estuarine Coastal and Shelf Science 48, 59–75.
Chen, C.T.A., Wang, S.L., 1999. Carbon, alkalinity and nutrient budgets on the East China Sea continental shelf. Journal of Geophysical Research—Oceans 104, 20675–20686.
Dugdale, R.C., Goering, J.J., 1967. Uptake of new and regenerated forms of nitrogen in primary productivity. Limnology and Oceanography 12, 196–206.
Efron, A., Gong, G., 1983. A leisurely look at the bootstrap, the jacknife, and cross-validation. American Statistician 37, 36–48.
Eppley, R.W., Peterson, B.J., 1979. Particulate organic-matter flux and planktonic new production in the deep ocean. Nature 282, 677–680.
Hama, T., Miyazaki, T., Ogawa, Y., Iwakuma, T., Takahashi, M., Otsuki, A., Ichimura, S., 1983. Measurement of photosynthetic production of a marine phytoplankton population using a stable ^{13}C isotope. Marine Biology 73, 31–36.
Han, I.S., Kamio, K., Matsuno, T., Manda, A., Isobe, A., 2001. High frequency current fluctuations and cross-shelf flows around the pycnocline near the shelf break in the East China Sea. Journal of Oceanography 57, 235–249.
Hashihama, F., Furuya, K., Kitajima, S., Takeda, S., Takemura, T., Kanda, J., 2009. Macro-scale exhaustion of surface phosphate by dinitrogen fixation in the western North Pacific. Geophysical Research Letters 36, L03610, http://dx.doi.org/10.1029/2008gl036866.
Isobe, A., Fujiwara, E., Chang, P.-H., Sugimatsu, K., Shimizu, M., Matsuno, T., Manda, A., 2004. Intrusion of less saline shelf water into the Kuroshio subsurface layer in the East China Sea. Journal of Oceanography 60, 853–863.
Kanda, J., Itoh, T., Ishikawa, D., Watanabe, Y., 2003. Environmental control of nitrate uptake in the East China Sea. Deep-sea Research Part II—Topical Studies in Oceanography 50, 403–422.
Kodama, T., Furuya, K., Hashihama, F., Takeda, S., Kanda, J., 2011. Occurrence of rain-origin nitrate patches at the nutrient-depleted surface in the East China Sea and the Philippine Sea during summer. Journal of Geophysical Research 116, C08003, http://dx.doi.org/10.1029/2010jc006814.
Kuroda, Y., Mitsudera, H., 1995. Observation of internal tides in the East-China-Sea with an underwater sliding vehicle. Journal of Geophysical Research-Oceans 100, 10801–10816.
Lee, J.H., Lozovatsky, I., Jang, S.T., Jang, C.J., Hong, C.S., Fernando, H.J.S., 2006. Episodes of nonlinear internal waves in the northern East China Sea. Geophysical Research Letters 33, L18601, http://dx.doi.org/10.1029/2006GL027136.
Liu, A.K., Chang, Y.S., Hsu, M.K., Liang, N.K., 1998. Evolution of nonlinear internal waves in the East and South China Seas. Journal of Geophysical Research-Oceans 103, 7995–8008.
Liu, K.K., Su, M.J., Hsueh, C.R., Gong, G.C., 1996. The nitrogen isotopic composition of nitrate in the Kuroshio Water northeast of Taiwan: evidence for nitrogen fixation as a source of isotopically light nitrate. Marine Chemistry 54, 273–292.
Marumo, R., Asaoka, O., 1974. *Trichodesmium* in the East China Sea. Journal of Oceanography 30, 298–303.
Matsuno, T., Hibiya, T., Kanari, S., Kobayashi, C., 1997. Small scale internal waves and turbulent fluctuations near the continental shelf break in the East China Sea. Journal of Oceanography 53, 259–269.
Matsuno, T., Lee, J.S., Shimizu, M., Kim, S.H., Pang, I.C., 2006. Measurements of the turbulent energy dissipation rate ε and an evaluation of the dispersion process of the Changjiang diluted water in the East China Sea. Journal of Geophysical Research111C11S09http://dxdoi.org/10.1029/2005jc003196.
Matsuno, T., Lee, J.S., Yanao, S., 2009. The Kuroshio exchange with the South and East China Seas. Ocean Science 5, 303–312.
Matsuno, T., Shimizu, M., Morii, Y., Nishida, H., Takaki, Y., 2005. Measurements of the turbulent energy dissipation rate around the shelf break in the East China Sea. Journal of Oceanography 61, 1029–1037.
McCarthy, J.J., Carpenter, E.J., 1983. Nitrogen cycling in near surface waters of the open ocean. In: Carpenter, E.J., Capone, D.G. (Eds.), Nitrogen in the Marine Environment. Academic Press, New York, pp. 487–572.
McCarthy, J.J., Garside, C., Nevins, J.L., 1999. Nitrogen dynamics during the Arabian Sea northeast monsoon. Deep-sea Research Part II—Topical Studies in Oceanography 46, 1623–1664.
McCarthy, J.J., Garside, C., Nevins, J.L., Barber, R.T., 1996. New production along 140 degrees W in the equatorial Pacific during and following the 1992 El Niño event. Deep-Sea Research Part II—Topical Studies in Oceanography 43, 1065–1093.
Minagawa, M., Ohashi, M., Kuramoto, T., Noda, N., 2001. $\delta^{15}N$ of PON and nitrate as a clue to the origin and transformation of nitrogen in the subarctic North Pacific and its marginal sea. Journal of Oceanography 57, 285–300.
Minagawa, M., Wada, E., 1986. Nitrogen isotope ratios of red tide organisms in the East-China-Sea—a characterization of biological nitrogen-fixation. Marine Chemistry 19, 245–259.
Montoya, J.P., Voss, M., Kahler, P., Capone, D.G., 1996. A simple, high-precision, high-sensitivity tracer assay for N_2 fixation. Applied and Environmental Microbiology 62, 986–993.
Mouriño-Carballido, B., Graña, R., Fernández, A., Bode, A., Varela, M., Domínguez, J. F., Escánez, J., de Armas, D., Marañón, E., 2011. Importance of N_2 fixation vs. nitrate eddy diffusion along a latitudinal transect in the Atlantic Ocean. Limnology and Oceanography 56, 999–1007, http://dx.doi.org/10.4319/lo.2011.56.3.0999.
Nakamura, T., Matsumoto, K., Uematsu, M., 2005. Chemical characteristics of aerosols transported from Asia to the East China Sea: an evaluation of anthropogenic combined nitrogen deposition in autumn. Atmospheric Environment 39, 1749–1758, http://dx.doi.org/10.1016/j.atmosenv.2004.11.037.
Nikurashin, N., Ferrari, R., 2010. Radiation and dissipation of internal waves generated by geostrophic motions impinging on small-scale topography: theory. Journal of Physical Oceanography 40, 1055–1074.
Niwa, Y., Hibiya, T., 2004. Three-dimensional numerical simulation of M2 internal tides in the East China Sea. Journal of Geophysical Research 109, C04027, http://dx.doi.org/10.1029/2003JC001923.
Osborn, T.R., 1980. Estimates of the local-rate of vertical diffusion from dissipation measurements. Journal of Physical Oceanography 10, 83–89.
Park, J.H., Andres, M., Martin, P.J., Wimbush, M., Watts, D.R., 2006. Second-mode internal tides in the East China Sea deduced from historical hydrocasts and a model. Geophysical Research Letters 33, L05602, http://dx.doi.org/10.1029/2005GL024732.
Sharples, J., Moore, C.M., Abraham, E.R., 2001. Internal tide dissipation, mixing, and vertical nitrate flux at the shelf edge of NE New Zealand. Journal of Geophysical Research 106, 14069–14081, http://dx.doi.org/10.1029/2000JC000604.
Shiozaki, T., Furuya, K., Kodama, T., Kitajima, S., Takeda, S., Takemura, T., Kanda, J., 2010. New estimation of N_2 fixation in the western and central Pacific Ocean and its marginal seas. Global Biogeochemical Cycles 24, GB1015, http://dx.doi.org/10.1029/2009GB003620.
Shiozaki, T., Furuya, K., Kodama, T., Takeda, S., 2009. Contribution of N_2 fixation to new production in the western North Pacific Ocean along 155°E. Marine Ecology—Progress Series 377, 19–32, http://dx.doi.org/10.3354/meps07837.
Shiozaki, T., Furuya, K., Kurotori, H., Kodama, T., Takeda, S., Endoh, T., Yoshikawa, Y., Ishizaka, J., Matsuno, T., 2011. Imbalance between vertical nitrate flux and nitrate assimilation on a continental shelf: implications of nitrification. Journal of Geophysical Research 116, C10031, http://dx.doi.org/10.1029/2010JC006934.
Stevens, C.L., Sutton, P.J.H., Law, C.S., 2012. Internal waves downstream of the Norfolk Ridge, western Pacific, and their biophysical implications. Limnology and Oceanography 57, 897–911, http://dx.doi.org/10.4319/lo.2012.57.4.0897.
Suzuki, R., Ishimaru, T., 1990. An improved method for the determination of phytoplankton chlorophyll using N, N-dimethylformamide. Journal of Oceanography 46, 190–194.
Yanagi, T., Shimizu, T., Lie, H.J., 1998. Detailed structure of the Kuroshio frontal eddy along the shelf edge of the East China Sea. Continental Shelf Research 18, 1039–1056.
Zhang, R., Chen, M., Cao, J., Ma, Q., Yang, J., Qiu, Y., 2012. Nitrogen fixation in the East China Sea and southern Yellow Sea during summer 2006. Marine Ecology Progress Series 447, 77–86, http://dx.doi.org/10.3354/meps09509.
Zhao, L., Guo, X., 2011. Influence of cross-shelf water transport on nutrients and phytoplankton in the East China Sea: a model study. Ocean Science 7, 27–43, http://dx.doi.org/10.5194/os-7-27-2011.